Fabricating metallic–dielectric zirconium nitride thin films for photoelectric conversion

Satoshi Ishii,[1,2,*] Anjaneyulu Oruganti,[3,4] Ilario Bisignano,[1,2] Hideki Abe[3]

[1] Research Center for Materials Nanoarchitectonics (MANA), National Institute for Materials Science (NIMS), 1-1 Namiki, Tsukuba, Ibaraki 305-0044 Japan.

[2] Faculty of Pure and Applied Physics, University of Tsukuba, Tsukuba, Ibaraki 305-8577 Japan.

[3] Center for Green Research on Energy and Environmental Materials, National Institute for Materials Science (NIMS), 1-1, Namiki, Tsukuba, Ibaraki, 305-0044 Japan

[4] Department of Chemistry, Central University of Karnataka, Kalaburagi, Karnataka, 585367 India.

*E-mail address: sishii@nims.go.jp

Keywords: zirconium nitride, thin film, permittivity, optical property, sputtering

Abstract

Metals and dielectrics are essential components in photoelectric conversions and plasmonics. In these applications, basically any materials with negative and positive permittivities can be used as metals and dielectrics, respectively. Although there are many possible combinations of metallic and dielectric materials, they usually consist of different elements, making it challenging to create metal-dielectric interfaces from materials with identical elements. In this study, metallic and dielectric zirconium nitrides (Zr-N) are fabricated by controlling the flow rates of argon and nitrogen. Characterization by X-ray photoemission spectroscopy and X-ray diffraction reveals that the metallic and dielectric phases are ZrN and Zr_3N_4, respectively. The photoresponse is demonstrated by constructing a metal–insulator–metal structure using metallic and dielectric Zr-N thin films. Fabricating plasmonic nanostructures in Zr-N thin films can potentially improve the photoresponse. Additionally, other transition metal nitrides are also candidates for realizing metallic and dielectric components with the same constituent elements.

Introduction

Metal and dielectric interfaces have been the major building blocks for photoelectric conversions and plasmonics[1, 2] including plasmonic metamaterials.[3] In photoelectric conversion at a metal-

dielectric interface, thermally non-equilibrium hot carriers, including hot holes and hot electrons, are excited by optical irradiation to the metal. These hot carriers are energetic such that they can be injected from the metal to dielectric if the photon energy is larger than the barrier height, which is typically smaller than the bandgap.[4-6] This significantly contrasts the optical excitation in semiconductors, where the excitation of electrons and holes only occurs when the incident photon energy is larger than the bandgap in the linear processes. As for plasmonics, surface plasmons are excited at a metal-dielectric interface. Photoelectric conversion processes, such as photodetection, photovoltaics, and photocatalysis can be enhanced by plasmon resonance. Typical materials that have so far been used for photoelectric conversion and plasmonics are gold, silver, and aluminum as metals, and silica, alumina, magnesium oxide, and titania as dielectrics. The materials listed above indicate that the compositions of the metals and dielectrics are typically different.

An important point to consider here is that metals used for photoelectric conversion and plasmonics do not need to be metals by the classification of materials science; any material with the negative real part of permittivity can be used as a metallic material to excite surface plasmons. For clarity, a material having negative permittivity is described as a metallic material hereafter. Indeed, there is a wide variety of metallic materials; transition metal nitrides,[7-9] transition metal carbides,[10-12] transparent conductive oxides,[8, 13] doped semiconductors,[14-19] two-dimensional materials including MXenes [20-22] and graphene.[23, 24] The use of non-metals for plasmonic photoelectric conversions and plasmonics has greatly expanded the research in this field.[9, 11]

Among the metallic materials introduced earlier, transition metal nitrides are among the few classes of materials that are metallic in the visible range. The carrier concentrations of transition metal nitrides are typically lower than those of noble metals, however, they showed better performance in generating hot carriers compared to noble metals.[25, 26] Within transition metal nitrides, zirconium nitride (ZrN) and titanium nitride (TiN) have been intensively studied because both Zr and Ti are abundant and have already been used in hard coatings for machine tools.[27] Upon comparison, ZrN is predicted to be more metallic than TiN.[28] ZrN is one of the phases in zirconium nitride (Zr-N) system; Zr_3N_4 is another phase which have been fabricated so far. Unlike ZrN, Zr_3N_4 is a dielectric with a bandgap of 2.3 to 3.17 eV.[29, 30] ZrN and Zr_3N_4 can be fabricated intentionally with reactive sputtering by controlling the gas flow rates of argon (Ar) and nitrogen (N_2). To date, most studies have focused on fabricating and characterizing individual Zr-N thin films. In contrast, in this study, ZrN and Zr_3N_4 were sequentially fabricated to form ZrN/Zr_3N_4/ZrN trilayers for photodetection. First, the sputtering conditions for fabricating ZrN and Zr_3N_4 were investigated, and their optical properties were characterized by transmittance measurements and spectroscopic ellipsometry. The crystal structure, chemical bonding, surface roughness, and electrical resistance were also investigated. Finally, the photoresponse of ZrN/Zr_3N_4/ZrN trilayers was demonstrated in the visible

range. This study shows that metallic and dielectric components can be fabricated from identical elements for photoelectric conversion, which has hardly been explored to date.

Method

Sample fabrication

All thin films were fabricated by DC magnetron sputtering (CFS-4EP-LL, Shibaura Mechatronics Co.) at room temperature where the target was 4-inch pure Zr and the DC power was 200 W. No post annealing was done for all the samples presented in this work. Borosilicate glass (EAGLE XG, Corning) and silicon wafer (Si; Wakatekku Co.) having a 100-nm thick oxide layer were used as substrates; the former and latter were mainly used for transmittance measurement and remaining characterizations, respectively. Five combinations of argon (Ar) and nitrogen (N_2) flow rates were tested to control the film properties. The deposition time was adjusted to aim 30 nm thickness. The gas flow rate and deposition time are listed in Table 1, and the five films were labeled as Zr-N-1, Zr-N-2, Zr-N-3, Zr-N-4, and Zr-N-5. The total gas flow rates were fixed at 28 SCCM for Zr-N-1, Zr-N-2, and Zr-N-3. The total gas flow rates for Zr-N-4 and Zr-N-5 were equal to or lower than 10 SCCM, and Zr-N-5 had a lower Ar flow rate than Zr-N-4 while keeping the identical N_2 flow rate. Note that 2 SCCM was the minimum flow rate for the sputtering system that was used. Trilayers of Zr-N-30 nm/Zr_3N_4 20 nm/Zr-N-40 nm were fabricated on a Si wafer having a 100-nm silicon dioxide using shadow masks following the reference,[31] which allowed the formation of interfaces without exposure to the atmosphere. The gas flow rates for top/bottom and middle layers were identical to Zr-N-3 and Zr-N-4, respectively. The trilayer samples can be considered as metal–insulator–metal (MIM) structure.

Table 1. Ar and N_2 gas flow rates, $N_2/(Ar+/N_2)$ ratio, and deposition times to sputter five Zr–N films.

	Zr-N-1	Zr-N-2	Zr-N-3	Zr-N-4	Zr-N-5
Ar/N_2 flow rate (SCCM)	21/7	14/14	7/21	8/2	6/2
$N_2/(Ar+N_2)$ ratio	0.25	0.5	0.75	0.2	0.25
Deposition time (s)	703	776	846	162	308

Characterization

The transmittance spectra were measured in the optical range (200-2000 nm) with a step size of 2 nm using a UV-VIS spectrometer (V-570, JASCO) where a blank port without any substrate was used as a reference for unity transmittance. Spectroscopic ellipsometry was performed with a SE 850, SENTECH Instruments GmbH. To fit psi and delta, Drude-Lorentz models were used in the fitting. The X-ray diffraction (XRD) patterns were measured by a SmartLab, Rigaku Co., which used Cu $K\alpha_1$ as an X-ray source. The scanning mode was 2-theta continuous scanning at 40 kV and 30 mA, incident slit was 1.0 mm, scanning step was 0.04 degrees. The XPS spectra were measured by HEA-4MS249 with 200 eV, 66 degrees in room temperature at the undulator BL15XU beam line of SPring-8, Japan. No sputtering ion beam species was used for the current XPS measurements. The surface roughness was characterized by the atomic force microscope function of a neaSCOPE (Attocube Systems AG). The sheet resistance was measured by the four-probe method using Keithley 2400 (TEKTRONIX, INC.) as a multimeter and a four-probe cable (SR4-SS, Astellatech, inc.). The photoresponse was measured by irradiating the sample with a wavelength-tunable light source (NIJI-2, Bunkoukeiki Co. Ltd.) and recording the current by a source meter (Keithley 2635, Tektronix, Inc.). No bias was applied during the photoresponse measurement. The I-V curve was measured with the same source meter.

Numerical electromagnetic simulations

The absorptance of the trilayers was numerically simulated using a software based on finite element method (COMSOL Multiphysics) where the permittivities obtained from the ellipsometry were used. The simulations were performed in two dimensions, and the actual thicknesses were used to define the geometry.

Results and discussion

Figure 1(a) shows a photo of the five films deposited on glass substrates. Apparently, while Zr-N-1, Zr-N-2, and Zr-N-3 are transparent, Zr-N-4 and Zr-N-5 are opaque. Figure 1(b) shows the transmittances of thin films. The transmittances of Zr-N-1, Zr-N-2, and Zr-N-3 are particularly high in the near-infrared (NIR) range. Zr-N-4 and Zr-N-5 are semi-transparent in the UV range and opacity is high in the NIR range. The results indicate that not only the Ar/N_2 flow rate ratio but also the total flow rate affected the properties.

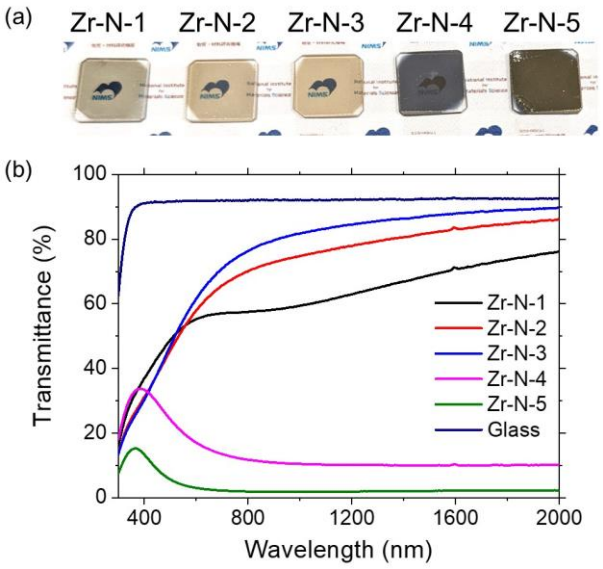

Figure 1. (a) Photo and (b) transmittance of the five Zr-N thin films deposited on glass substrates, along with the spectrum of the bare glass substrate.

To further elucidate the optical properties of the thin films, in Figure 2 the real and imaginary parts of complex permittivity are plotted. For Zr-N-1, Zr-N-2, and Zr-N-3, the real parts are positive, indicating that they are dielectric. The imaginary parts are low in the visible and NIR regions and their values decreased in the numerical order of sample name. This is consistent with the transmittance which increases in numerical order of the sample name as shown in Figure 1(b). The low transmittance in the UV range can be explained by the large imaginary parts in the UV range. In contrast to the above three thin films, the real parts of Zr-N-4 and Zr-N-5 are negative, which is characteristic of metals. As the imaginary parts of Zr-N-4 and Zr-N-5 are comparable, a larger real part in the negative direction for Zr-N-5 than for Zr-N-4 resulted in lower transmittance, which is consistent with the measured transmittance shown in Figure 1(b). Also, the positive real parts in the UV range explain semi-transparency in the UV range. The optical characterizations have elucidated that dielectric Zr-N and metallic Zr-N can be fabricated by merely changing the gas flow rate of Ar and N_2. Specifically, using a total gas flow rate of 28 SCCM and ≤10 SCCM resulted in dielectric and metallic thin films, respectively, whereas reducing the Ar flow rate renders the thin films more metallic. Note that the ellipsometry technique employed in the current study only provided averaged permittivities within the beam spot of the ellipsometer. To elucidate the nanoscale homogeneity of the thin films, a scattering-type scanning near-field optical microscope can be used.[32]

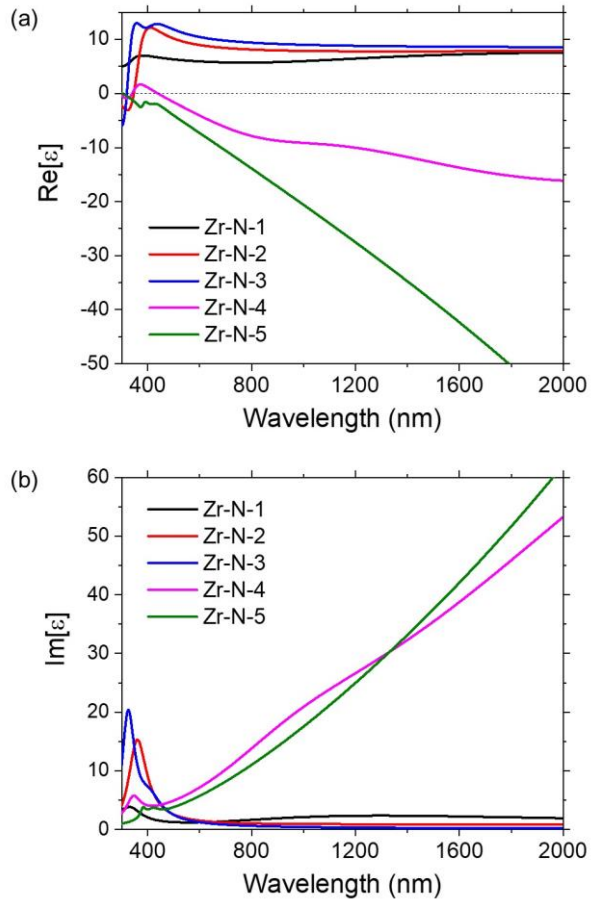

Figure 2. (a) Real and (b) imaginary parts of the complex permittivities of the five Zr-N thin films deposited on Si wafers.

To characterize the material properties of Zr-N thin films, the XRD patterns and XPS spectra of N 1s and Zr 3d are shown in Figure 3(a), 3(b) and 3(c), respectively. The XRD patterns of Zr-N-4 and Zr-N-5 clearly show (111), (200), (220), and (311) peaks of cubic ZrN phase.[29, 33] For Zr-N-1, Zr-N-2 and Zr-N-3, the above mentioned ZrN peaks are weak and becomes less obvious in numerical order of the sample name. Conversely, on the lower angle side of ZrN(111) peak, a shallow peak grows in numerical order of the sample name, which can be assigned to orthorhombic Zr_3N_4(320) peak.[34] The XPS analysis confirms the results of XRD analysis as follows. For the case of N 1s spectra shown in Figure 3(b), while Zr-N-1, Zr-N-2, and Zr-N-3 have dominant peaks at 395-396 eV which are associated to Zr_3N_4 phase, Zr-N-4 and Zr-N-5 have dominant peaks at ~397 eV which are associated to ZrN phase.[35-37] For the case of Zr 3d spectra shown in Figure 3(c), Zr-N-1, Zr-N-2 and Zr-N-3 have two dominant peaks at ~179.5 eV and ~182 eV, and these two peaks shift to lower binding energy for Zr-N-4 and Zr-N-5. These peak shifts can be attributed to the Zr_3N_4 phase

in Zr-N-1, Zr-N-2 and Zr-N-3 and ZrN phase in Zr-N-4 and Zr-N-5.[36] Considering the above XRD and XPS analyses, it is plausible that Zr-N-1, Zr-N-2 and Zr-N-3 are dielectric because they have a Zr_3N_4 phase, and Zr-N-4 and Zr-N-5 are metallic because they have a ZrN phase. In addition, the O 1s XPS spectra of the five samples are plotted in Figure S1. The main peaks at 529.5-530 eV are due to the presence of ZrO_2, which indicates that the films were slightly oxidized.[38, 39] The peak at 532 eV for Zr-N-3 is due to the absorbed oxygen.[39] Although oxygen existed in the samples, the oxygen concentrations were considered low as oxygen-related peaks did not appear in the XRD patterns, and Zr-N-4 and Zr-N-5 became metallic, which cannot happen with large oxygen concentrations.

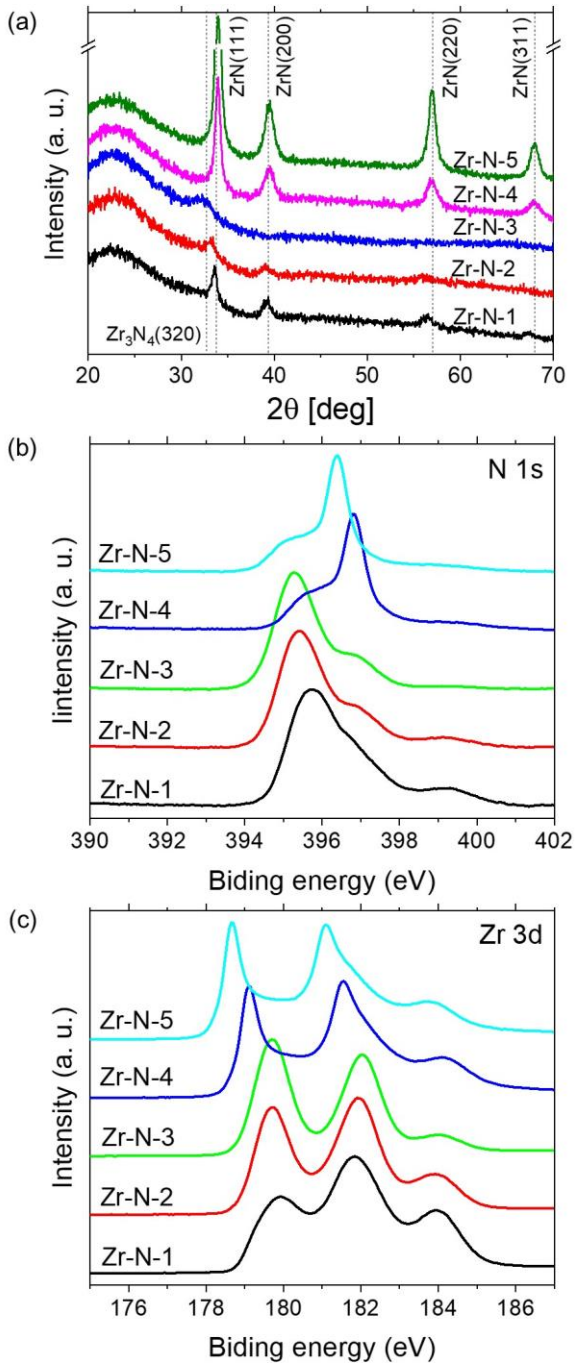

Figure 3. (a) XRD patterns and (b) XPS N 1s and (c) XPS Zr 3d spectra for the five Zr-N thin films.

Electrical resistance and route mean square (RMS) surface roughness calculated from the AFM images in Figure S2 results are summarized in Table 2. Electrical resistance measurements revealed that while Zr-N-1, Zr-N-2 and Zr-N-3 have higher resistance, Zr-N-4 and Zr-N-5 have lower resistance. The resistance values coincide with the dielectric and metallic properties of the samples.

Despite differing in their material properties, all the samples have roughness values below 1 nm, indicating smooth surfaces.

Table 2. Sheet resistance and surface roughness of the five Zr-N thin films.

	Zr-N-1	Zr-N-2	Zr-N-3	Zr-N-4	Zr-N-5
Sheet resistance (Ω/□)	2.4×10^{8}	$>1.7\times10^{9}$	$>1.7\times10^{9}$	1.8×10^{5}	31
Surface roughness (nm)	0.50	0.87	0.77	0.64	0.64

Finally, the photoresponse of ZrN/Zr_3N_4/ZrN trilayers was evaluated. As a representative example, Figure 4(a) shows the time-dependent responsivity of the sample at 800 nm wavelength. As the light source was turned on every five seconds, clear photoresponse was recorded. As the bandgap of Zr_3N_4 is at least larger than 2.3 eV,[29] the hot carriers excited in ZrN were considered to be the major photo-carriers. Responsivity was recorded at other wavelengths and its wavelength dependence is plotted in Fig. 4(b). The responsivity does not show a monotonic decrease with respect to wavelength increase, and is the smallest at 500 nm. To elucidate the wavelength dependence, I-V measurement was performed as shown in Figure S3, and the ZrN/Zr_3N_4 interfaces were considered to be ohmic from the straight I-V curve. For an ohmic contact, responsivity is known to be proportional to the integrated absorptance where the integration range is the electron mean free path (MFP) in the metallic material.[25, 40] Note that as the top ZrN layer was semi-transparent, the difference in integrated absorptance between the top and bottom ZrN layers mattered. As the MFP of ZrN was reported to be on the order of unity nanometers,[41-44] here the MFP was set at 5 nm and the absorptance of the top and bottom ZrN layers was integrated for 5 nm from each interface. The difference in integrated absorptance between the top and bottom ZrN layers is also plotted in Fig. 4(b). The absorptance difference was also simulated assuming 10-nm MFP, and the wavelength dependence was similar to that of 5-nm MFP as shown in Figure S4. The overall wavelength dependences of responsivity and absorptance difference reasonably agree, both having the minimum values around 500 nm. Thus, the wavelength dependence of responsivity can be roughly explained by the difference in absorptance difference between the top and bottom ZrN layers. A possible reason for the discrepancy between the two is the slight absorption in the Zr_3N_4 layer in the experiment, which was not considered in our simplified analysis. One way to improve the responsivity is to pattern the top layer and tune the middle layer thickness to excite strong plasmon resonances.[45]

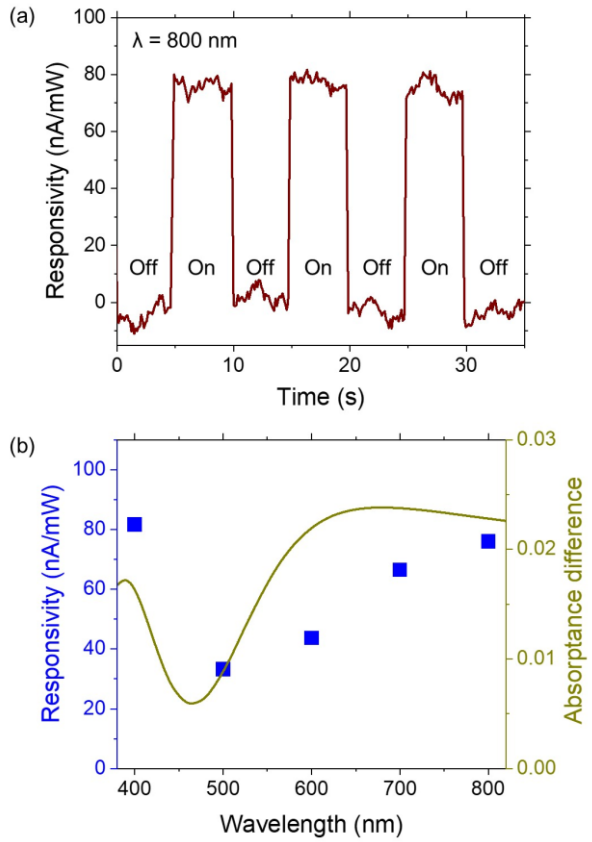

Figure 4. (a) Time dependent responsivity of the trilayers irradiated at 800 nm wavelength. The light source was turned on every five seconds. (b) Wavelength dependent responsivity of the trilayers and simulated absorptance difference between the top and bottom ZrN layers. The absorptance was integrated for 5 nm from each interface.

The current work demonstrates that photoresponsive MIM structures can be fabricated with Zr-N thin films without using other materials. With the nanofabrication of metallic and dielectric Zr-N thin films, plasmonic photocatalytic structures and plasmonic photovoltaic devices may also be fabricated. In addition, other transition metal nitride systems such as titanium-nitride and hafnium-nitride can also be explored to fabricate dielectric and metallic thin films selectively. Using identical elements to fabricate metallic and dielectric components is attractive for fabrication purposes and will widen the material choice for exploring novel functionalities.

Conclusion

To summarize, Zr-N thin films were fabricated using DC magnetron sputtering with varying Ar/N_2 flow rates. The films were characterized through UV-VIS spectroscopy, ellipsometry, XRD, XPS, four-probe measurements, and AFM. When the total flow rate was 28 SCCM and N_2 ratio was 25%

or more, the thin films displayed a Zr_3N_4 phase and dielectric optical properties. When the total flow rates were 10 SCCM or lower and an N_2 ratio was 25% or less, the thin films exhibited a ZrN phase with metallic optical properties. Regardless of the gas flow rate, the RMS surface roughness remained below 1 nm. An MIM trilayer sample was fabricated with metallic Zr-N films at the top and bottom and a dielectric Zr-N film in the middle. The photoelectric conversion was examined in the visible range, revealing a clear photoresponse when the visible light source was turned on. The overall wavelength dependence of the responsivity can be explained by the integrated absorptance difference between the top and bottom layers, with the integration range within the MFP. Since the responsivity is proportional to absorptance, exciting surface plasmon resonance in the nanostructures could significantly enhance the responsivity.

ORCID
Satoshi Ishii: 0000-0003-0731-8428
Oruganti Anjaneyulu: 0000-0002-1505-7195
Ilario Bisignano: 0009-0004-9964-2106
Hideki Abe: 0000-0002-8392-7586

Supporting Information
XPS spectra of O 1s, AFM images, I-V curve, and wavelength-dependent absorptance difference of trilayers.

Acknowledgment
S.I. acknowledges the financial support from JST FOREST (JPMJFR2139) and Kakenhi from JSPS (22H01917), Japan.

Data availability statement
All data that support the findings of this study are included within the article.

Additional information
Supplementary information is available online.

References
1. Raether, H., Surface plasmons on smooth surfaces. *Surface plasmons on smooth and rough surfaces and on gratings* **2006**, 4-39.
2. Maier, S. A., *Plasmonics: fundamentals and applications*. Springer: 2007; Vol. 1.

3. Shvets, G.; Tsukerman, I., *Plasmonics and Plasmonic Metamaterials*. 2011.
4. Linic, S.; Christopher, P.; Ingram, D. B., Plasmonic-metal nanostructures for efficient conversion of solar to chemical energy. *Nat. Mater.* **2011,** *10* (12), 911-921.
5. Clavero, C., Plasmon-induced hot-electron generation at nanoparticle/metal-oxide interfaces for photovoltaic and photocatalytic devices. *Nat. Photon.* **2014,** *8* (2), 95-103.
6. Brongersma, M. L.; Halas, N. J.; Nordlander, P., Plasmon-induced hot carrier science and technology. *Nat. Nanotechnol.* **2015,** *10* (1), 25-34.
7. Steinmüller-Nethl, D.; Kovacs, R.; Gornik, E.; Rödhammer, P., Excitation of surface plasmons on titanium nitride films: determination of the dielectric function. *Thin Solid Films* **1994,** *237* (1), 277-281.
8. Naik, G. V.; Kim, J.; Boltasseva, A., Oxides and nitrides as alternative plasmonic materials in the optical range. *Opt. Mater. Express* **2011,** *1* (6), 1090-1099.
9. Naik, G. V.; Shalaev, V. M.; Boltasseva, A., Alternative Plasmonic Materials: Beyond Gold and Silver. *Adv. Mater.* **2013,** *25* (24), 3264-3294.
10. Bonnot, A. M.; Belkhir, H.; Pailharey, D.; Mathiez, P., Reactively sputtered zirconium carbides, carbonitrides and nitrides thin films-optical properties. *Sol. Energy Mater.* **1986,** *14* (3), 375-384.
11. Ishii, S.; Shinde, S. L.; Nagao, T., Nonmetallic Materials for Plasmonic Hot Carrier Excitation. *Adv. Opt. Mater.* **2019,** *7* (1), 1800603.
12. Lan, L.; Fan, X.; Gao, Y.; Li, G.; Hao, Q.; Qiu, T., Plasmonic metal carbide SERS chips. *J. Mater. Chem. C* **2020,** *8* (41), 14523-14530.
13. West, P. R.; Ishii, S.; Naik, G. V.; Emani, N. K.; Shalaev, V. M.; Boltasseva, A., Searching for better plasmonic materials. *Laser Photonics Rev.* **2010,** *4* (6), 795-808.
14. Hoffman, A. J.; Alekseyev, L.; Howard, S. S.; Franz, K. J.; Wasserman, D.; Podolskiy, V. A.; Narimanov, E. E.; Sivco, D. L.; Gmachl, C., Negative refraction in semiconductor metamaterials. *Nat. Mater.* **2007,** *6* (12), 946-950.
15. Cleary, W. J.; Peale, E. R.; Shelton, D.; Boreman, G.; Soref, R.; Buchwald, R. W., Silicides for infrared surface plasmon resonance biosensors. *MRS Online Proceedings Library* **2009,** *1133* (1), 1003.
16. Cleary, J. W.; Peale, R. E.; Shelton, D. J.; Boreman, G. D.; Smith, C. W.; Ishigami, M.; Soref, R.; Drehman, A.; Buchwald, W. R., IR permittivities for silicides and doped silicon. *J. Opt. Soc. Am. B* **2010,** *27* (4), 730-734.
17. Blaber, M. G.; Arnold, M. D.; Ford, M. J., A review of the optical properties of alloys and intermetallics for plasmonics. *J. Condens. Matter Phys.* **2010,** *22* (14), 143201.
18. Ginn, J. C.; Jarecki, R. L., Jr.; Shaner, E. A.; Davids, P. S., Infrared plasmons on heavily-

doped silicon. *J. Appl. Phys.* **2011,** *110* (4).
19. Shahzad, M.; Medhi, G.; Peale, R. E.; Buchwald, W. R.; Cleary, J. W.; Soref, R.; Boreman, G. D.; Edwards, O., Infrared surface plasmons on heavily doped silicon. *J. Appl. Phys.* **2011,** *110* (12).
20. El-Demellawi, J. K.; Lopatin, S.; Yin, J.; Mohammed, O. F.; Alshareef, H. N., Tunable Multipolar Surface Plasmons in 2D Ti3C2Tx MXene Flakes. *ACS Nano* **2018,** *12* (8), 8485-8493.
21. Velusamy, D. B.; El-Demellawi, J. K.; El-Zohry, A. M.; Giugni, A.; Lopatin, S.; Hedhili, M. N.; Mansour, A. E.; Fabrizio, E. D.; Mohammed, O. F.; Alshareef, H. N., MXenes for Plasmonic Photodetection. *Adv. Mater.* **2019,** *31* (32), 1807658.
22. Jakšić, Z.; Obradov, M.; Jakšić, O.; Tanasković, D.; Radović, D. V. In *Reviewing MXenes for Plasmonic Applications: Beyond Graphene*, 2019 IEEE 31st International Conference on Microelectronics (MIEL), 16-18 Sept. 2019; 2019; pp 91-94.
23. Chen, J.; Badioli, M.; Alonso-González, P.; Thongrattanasiri, S.; Huth, F.; Osmond, J.; Spasenović, M.; Centeno, A.; Pesquera, A.; Godignon, P.; Zurutuza Elorza, A.; Camara, N.; de Abajo, F. J. G.; Hillenbrand, R.; Koppens, F. H. L., Optical nano-imaging of gate-tunable graphene plasmons. *Nature* **2012,** *487* (7405), 77-81.
24. Farhat, M.; Guenneau, S.; Bağcı, H., Exciting Graphene Surface Plasmon Polaritons through Light and Sound Interplay. *Phys. Rev. Lett.* **2013,** *111* (23), 237404.
25. Ishii, S.; Shinde, S. L.; Jevasuwan, W.; Fukata, N.; Nagao, T., Hot Electron Excitation from Titanium Nitride Using Visible Light. *ACS Photonics* **2016,** *3* (9), 1552-1557.
26. Naldoni, A.; Guler, U.; Wang, Z.; Marelli, M.; Malara, F.; Meng, X.; Besteiro, L. V.; Govorov, A. O.; Kildishev, A. V.; Boltasseva, A.; Shalaev, V. M., Broadband Hot-Electron Collection for Solar Water Splitting with Plasmonic Titanium Nitride. *Adv. Opt. Mater.* **2017,** *5* (15), 1601031.
27. Chhowalla, M.; Unalan, H. E., Thin films of hard cubic Zr3N4 stabilized by stress. *Nat. Mater.* **2005,** *4* (4), 317-322.
28. Kumar, M.; Umezawa, N.; Ishii, S.; Nagao, T., Examining the performance of refractory conductive ceramics as plasmonic materials: a theoretical approach. *ACS Photonics* **2016,** *3* (1), 43-50.
29. Signore, M. A.; Valerini, D.; Tapfer, L.; Caretto, G.; Rizzo, A., Zirconium nitride films deposited in ($Ar + N_2 + H_2$) sputtering atmosphere: Optical, structural, and electrical properties. *J. Vac. Sci. Technol. A* **2011,** *29* (6).
30. Rizzo, A.; Signore, M. A.; Mirenghi, L.; Tapfer, L.; Piscopiello, E.; Salernitano, E.; Giorgi, R., Sputtering deposition and characterization of zirconium nitride and oxynitride

films. *Thin Solid Films* **2012,** *520* (9), 3532-3538.
31. Shinde, S. L.; Ishii, S.; Nagao, T., Sub-Band Gap Photodetection from the Titanium Nitride/Germanium Heterostructure. *ACS Appl. Mater. Interfaces* **2019,** *11* (24), 21965-21972.
32. Stanciu, S. G.; Tranca, D. E.; Pastorino, L.; Boi, S.; Song, Y. M.; Yoo, Y. J.; Ishii, S.; Hristu, R.; Yang, F.; Bussetti, G.; Stanciu, G. A., Characterization of Nanomaterials by Locally Determining Their Complex Permittivity with Scattering-Type Scanning Near-Field Optical Microscopy. *ACS Appl. Nano Mater.* **2020,** *3* (2), 1250-1262.
33. Benia, H. M.; Guemmaz, M.; Schmerber, G.; Mosser, A.; Parlebas, J. C., Optical and electrical properties of sputtered ZrN compounds. *Catal. Today* **2004,** *89* (3), 307-312.
34. Carvalho, P.; Vaz, F.; Rebouta, L.; Cunha, L.; Tavares, C. J.; Moura, C.; Alves, E.; Cavaleiro, A.; Goudeau, P.; Le Bourhis, E.; Rivière, J. P.; Pierson, J. F.; Banakh, O., Structural, electrical, optical, and mechanical characterizations of decorative ZrOxNy thin films. *J. Appl. Phys.* **2005,** *98* (2).
35. Prieto, P.; Galan, L.; Sanz, J., Electronic structure of insulating zirconium nitride. *Phys. Rev. B* **1993,** *47* (3), 1613.
36. Del Re, M.; Gouttebaron, R.; Dauchot, J.-P.; Leclère, P.; Terwagne, G.; Hecq, M., Study of ZrN layers deposited by reactive magnetron sputtering. *Surf. Coat. Technol.* **2003,** *174*, 240-245.
37. Rizzo, A.; Signore, M.; Mirenghi, L.; Serra, E., Properties of ZrNx films with x> 1 deposited by reactive radiofrequency magnetron sputtering. *Thin Solid films* **2006,** *515* (4), 1307-1313.
38. Wiame, H.; Centeno, M.-A.; Picard, S.; Bastians, P.; Grange, P., Thermal oxidation under oxygen of zirconium nitride studied by XPS, DRIFTS, TG-MS. *J. Eur. Ceram. Soc.* **1998,** *18* (9), 1293-1299.
39. Matsuoka, M.; Isotani, S.; Sucasaire, W.; Kuratani, N.; Ogata, K., X-ray photoelectron spectroscopy analysis of zirconium nitride-like films prepared on Si(100) substrates by ion beam assisted deposition. *Surf. Coat. Technol.* **2008,** *202* (13), 3129-3135.
40. Zheng, B. Y.; Zhao, H.; Manjavacas, A.; McClain, M.; Nordlander, P.; Halas, N. J., Distinguishing between plasmon-induced and photoexcited carriers in a device geometry. *Nat. Commun.* **2015,** *6* (1), 7797.
41. Debessai, M.; Filip, P.; Aouadi, S. M., Niobium zirconium nitride sputter-deposited protective coatings. *Appl. Surf. Sci.* **2004,** *236* (1), 63-70.
42. Bazhanov, D. I.; Knizhnik, A. A.; Safonov, A. A.; Bagatur'yants, A. A.; Stoker, M. W.; Korkin, A. A., Structure and electronic properties of zirconium and hafnium nitrides and

oxynitrides. *J. Appl. Phys.* **2005,** *97* (4), 044108.

43. Sandu, C. S.; Medjani, F.; Sanjinés, R., Optical and electrical properties of sputtered Zr-Si-N thin films: from solid solution to nanocomposite. *Rev. Adv. Mater. Sci* **2007,** *15*, 173-178.
44. Veszelie, M.; Andersson, K. E.; Roos, A., Optical characterization of sputtered semitransparent zirconium nitride films. *Opt. Mater.* **1993,** *2* (4), 257-266.
45. Li, W.; Guler, U.; Kinsey, N.; Naik, G. V.; Boltasseva, A.; Guan, J.; Shalaev, V. M.; Kildishev, A. V., Refractory Plasmonics with Titanium Nitride: Broadband Metamaterial Absorber. *Adv. Mater.* **2014,** *26* (47), 7959-7965.

Graphic for manuscript